Exploring Structural Signatures of the Lanthipeptide Prochlorosin 2.8 using Tandem Mass Spectrometry and Trapped Ion Mobility-Mass Spectrometry

Kevin Jeanne Dit Fouque,^{1,2,#} Julian D. Hegemann,^{3,#} Miguel Santos-Fernandez,¹ Tung T.

Le,⁴ Mario Gomez-Hernandez,¹ Wilfred A. van der Donk,⁴ and Francisco Fernandez
Lima*,^{1,2}

¹ Department of Chemistry and Biochemistry, Florida International University, 11200 SW 8th Street,
Miami, FL 33199, United States.

² Biomolecular Science Institute, Florida International University, 11200 SW 8th Street, Miami, FL 33199,
United States.

³ Institute of Chemistry, Technische Universität Berlin, Straße des 17. Juni 135, 10623 Berlin, Germany.

⁴ Department of Chemistry and Howard Hughes Medical Institute, University of Illinois at Urbana-Champaign, 600 South Mathews Avenue, Urbana, IL 61801, United States.

Address reprint requests to Dr. Francisco Fernandez-Lima; Address: 11200 SW 8th Street, AHC4-233, Miami, FL 33199, United States; Telephone: +1 305-348-2037; E-mail: fernandf@fiu.edu

ABSTRACT

Lanthipeptides are a family of ribosomally synthesized and post-translationally modified peptides (RiPPs) characterized by intramolecular thioether cross-links formed between a dehydrated serine/threonine (dSer/dThr) and a cysteine residue. Prochlorosin 2.8 (Pcn2.8) is a class II lanthipeptide that exhibits a non-overlapping thioether ring pattern, for which no biological activity has been reported yet. The variant Pcn2.8[16RGD] has been shown to bind tightly to the ανβ3 integrin receptor. In the present work, tandem mass spectrometry, using collision induced dissociation (CID) and electron capture dissociation (ECD), and trapped ion mobility spectrometry - mass spectrometry (TIMS-MS), were used to investigate structural signatures for the non-overlapping thioether ring pattern of Pcn₂.8. CID experiments on Pcn₂.8 yielded b_i and y_i fragments between the thioether cross-links, evidencing the presence of a non-overlapping thioether ring pattern. ECD experiments of Pcn2.8 showed a significant increase of hydrogen migration events near the residues involved in the thioether rings with a more pronounced effect at the dehydrated residues as compared to the cysteine residues. The high-resolution mobility analysis, aided by site-directed mutagenesis ([P8A], [P11A], [P12A], [P8A/P11A], [P8A/P12A], [P11A/P12A] and [P8A/P11A/P12A] variants), demonstrated that Pcn2.8 adopts cis/trans-conformations at Pro8, Pro11 and Pro12 residues. These observations were found complementary to recent NMR findings, for which only the Pro8 residue was evidenced to adopt *cis/trans*-orientations. This study highlights the analytical power of the TIMS-MS/MS workflow for the structural characterization of lanthipeptides and could be a useful tool in our understanding of the biologically important structural elements that drive the thioether cyclization process.

Keywords: Pcn2.8, lanthipeptide, thioether cross-link, *cis/trans*-configuration, collision induced dissociation, electron capture dissociation, trapped ion mobility spectrometry.

1. INTRODUCTION

Lanthipeptides are a structurally unique class of ribosomally synthesized and posttranslationally modified peptides (RiPPs) that display various biological activities, including antimicrobial, antifungal, morphogenetic, antiviral, antinociceptive, and antiallodynic properties [1,2]. Lanthipeptides are characterized by intramolecular β thioether cross-links, called (methyl)lanthionines ((Me)Lan), formed between a dehydrated serine (dSer) or threonine (dThr) residue and a cysteine residue through the action of lanthipeptide synthetases (Figure 1a) [1-3]. The thioether cross-links are generated by a 1,4-Michael addition between the thiol group of the cysteine residue and the β-carbon of the dehydrated residue (Figure 1a) [2]. The lanthipeptide family is divided into five classes depending on the dehydratation process (Figure 1b) [2-6]. Many lanthipeptides were discovered through genome-mining approaches and isolation of new lanthipeptide structures as well as generation of lanthipeptide libraries are an active area of research [7-16]. The utility of β -thioether cross-links for stabilizing lanthipeptides, both natural and designed, together with their panel of biological activities, makes them a promising scaffold for next-generation drug design [17-23]. However, altered lanthipeptide synthetases can result in different thioether ring patterns (Figure S1) [24,25], making their characterization not readily accessible using traditional structural biology tools. Thus, the discovery and design of new lanthipeptides as well as generation of lanthipeptide libraries as potential drug candidates require analytical tools capable of unambiguously and rapidly characterizing the lanthipeptide ring topologies.

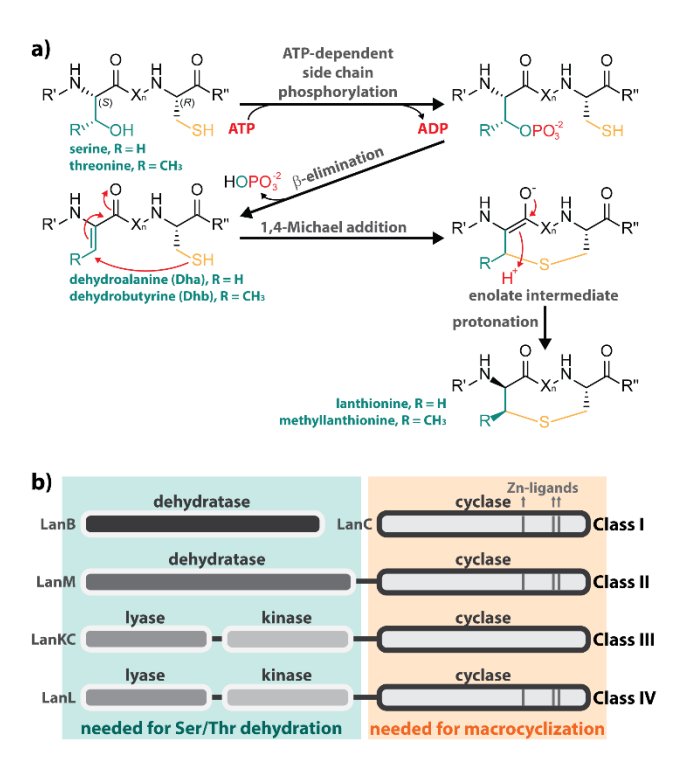


Figure 1. (a) Mechanisms of the lanthipeptide biosynthesis, starting with a dehydratation of Ser/Thr residues, followed by a cyclization through nucleophilic attack of Cys thiol groups. (b) General classification of lanthipeptide processing enzymes. The details of the recently reported class V lanthipeptides have not yet been worked out.

Prochlorosins are class II lanthipeptides produced by *Prochlorococcus* MIT 9313, which harbors multiple genes encoding ProcA precursor peptides but only a single gene encoding the lanthipeptide synthetase ProcM [2,26,27]. Among them, prochlorosin 2.8 (Pcn2.8) is a 19 residue lanthipeptide characterized by a non-overlapping thioether ring pattern (Figure 2) [28]. The intramolecular thioether cross-links are generated between Cys3 (highlighted in orange in Figure 2) and dSer9 (highlighted in green in Figure 2) residues as well as between dSer13 (highlighted in green in Figure 2) and Cys19 (highlighted in orange in Figure 2) residues. To date, no biological activity has been reported for Pcn2.8. However, an engineered variant, Pcn2.8[16RGD], has been demonstrated to tightly bind to the α v β 3 integrin receptor [28].

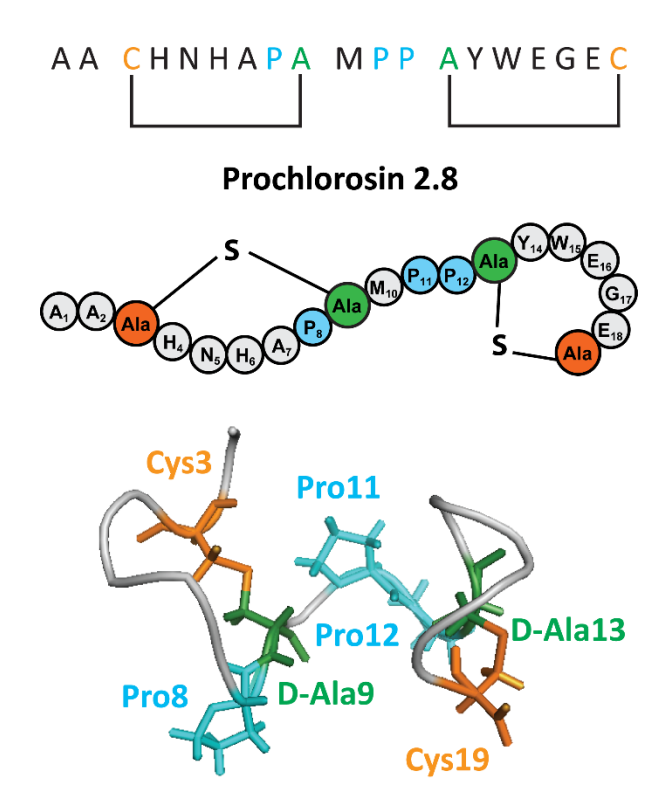


Figure 2. Sequence, schematic and 3D representation (pdb: 6VLJ [29]) of the lanthipeptide prochlorosin 2.8. The Cys and dSer residues, involved in the thioether cross-link formation, are colored in orange and green, respectively. The Pro residues are highlighted in blue.

Modern nuclear magnetic resonance (NMR) spectroscopy is a method of choice for the comprehensive characterization of lanthipeptides and assignment of the ring patterns, as illustrated by several reported structures [2,4,27,29-39]. NMR studies on Pcn2.8 revealed a non-overlapping ring pattern as well as the presence of both *cis*- and *trans*-orientations at the Pro8 residue, with the major structure a *cis*-conformation, while Pro11 and Pro12 residues only exhibited nuclear Overhauser effects (NOE) characteristic of *trans*-conformations [29]. Due to the relatively large amount of sample required for NMR studies, the ring patterns of most other prochlorosins have only been predicted based on tandem mass spectrometry (MS/MS) using collision induced dissociation (CID) [25,28,40]. As the presence of a thioether cross-link prohibits cleavage inside the ring, this MS/MS approach is useful for lanthipeptide ring assignment since different fragmentation patterns would be observed for non-overlapping and overlapping ring topologies [25]. Pcn2.8 generates fragments between dSer9 (highlighted in green in Figure 2) and dSer13 (highlighted in green in Figure 2) residues,

evidencing a non-overlapping ring pattern using CID [25,28]. Other complementary MS-based techniques, including electron capture dissociation (ECD) and ion mobility spectrometry – mass spectrometry (IMS-MS), were demonstrated to be very efficient alternate strategies for the structural characterization and pattern assignment for other RiPPs, such as lasso peptides [41-46].

In the present work, the lanthipeptide Pcn2.8 (Figure 2) was investigated using tandem mass spectrometry (CID and ECD) and trapped ion mobility spectrometry – mass spectrometry (TIMS-MS). The CID and ECD fragmentation patterns as well as mobility profiles were probed to evidence a non-overlapping ring pattern for Pcn2.8. In addition, the *cis/trans*-proline orientations at Pro8, Pro11 and Pro12 residues in Pcn2.8 (highlighted in blue in Figure 2) were studied using CID, ECD and TIMS-MS in combination with site-directed mutagenesis, involving [P8A], [P11A], [P12A], [P8A/P11A], [P8A/P12A], [P11A/P12A] and [P8A/P11A/P12A] variants, for direct comparison with recently reported NMR studies.

2. EXPERIMENTAL SECTION

2.1. Peptides and Sample Preparation. Details on production of Pcn2.8 and its variants have been previously described [28]. Briefly, we employed a small scale expression protocol using *E. coli* BL21(DE3) carrying a pRSF Duet plasmid that encodes His6-tagged ProcA2.8 (or variants thereof) and untagged ProcM. Production was accomplished by expression in 100 mL of lysogeny broth (LB) medium using 50 µg/mL kanamycin as selection marker. Expression cultures were inoculated 1:100 with a 37 $^{\circ}\text{C}$ LB overnight culture and then grown at 37 °C. When the optical density at 600 nm (OD600) reached ~0.4-0.5, the culture flasks were moved to another culture shaker at 18 °C, shaken for another 1 h, and then induced by adding 20 μL of a 0.5 M stock solution of isopropyl β-D-1-thiogalactopyranoside (IPTG, final concentration 0.1 mM) at an OD600 of ~0.5-0.7. Expression was carried out overnight at 18 °C. The next morning, 15 mL aliquots of the cultures were harvested by centrifugation. The modified His6-ProcA2.8 precursor and variants thereof were isolated by resuspending cell pellets in 1 mL of guanidinium chloride lysis buffer (500 mM NaCl, 20 mM phosphate, 6 M guanidinium chloride, 0.5 mM imidazole, pH 7.5), lysing them at RT using a Vibra Cell sonicator (Sonics & Materials) with a microtip (settings: 40% amplitude, 30 s total

sonication time alternating between 2 s on- and 2 s off-pulse), and then performing microscale NiNTA chromatography. For the latter, the lysates were cleared by centrifugation (RT, 20 min, 15700g) and transferred to fresh 2 mL microreaction tubes. Next, 180 µL of NiNTA resin (prequilibrated by washing twice with the guanidinium chloride lysis buffer) were added, and samples were incubated at RT for 30 min while slowly shaking. Samples were then loaded onto empty microbiospin chromatography columns (BioRad) and centrifuged at 270g until all liquid had passed through. The retained resin was washed twice. First by resuspending the resin with 800 µL of guanidinium chloride wash buffer (500 mM NaCl, 20 mM phosphate, 4 M guanidinium chloride, 30 mM imidazole, pH 7.5). Then, after again removing the liquid by centrifugation at 270g, by resuspending the resin with 800 µL of a PBS wash buffer (300 mM NaCl, 20 mM phosphate, 30 mM imidazole, pH 7.5). After centrifugation at 270g until all liquid was removed, the columns were transferred to fresh 2 mL microreaction tubes and eluted with 500 µL of a PBS elution buffer (300 mM NaCl, 20 mM phosphate, 500 mM imidazole, 1 mM tris(2-carboxyethyl)phosphine, pH 7.5). For the elution, the resin was resuspended on the column in the elution buffer and incubated for 5 min at RT, before centrifugation at 270g until all liquid passed into the collection tube. For release of the modified core peptide, the elution fraction were incubated with LahT(150) as described previously [28,47]. The [P8A], [P11A], [P12A], [P8A/P11A], [P8A/P12A], [P11A/P12A] and [P8A/P11A/P12A] variants of Pcn2.8 were produced by site-directed ligase-independent mutagenesis (SLIM) on the expression plasmid his₆procA2.8(G-1K)[MCS1]:procM[MCS2] pRSF following standard protocols [48,49]. The lanthipeptides were subjected to C₁₈ Zip Tip (Millipore, Burlington, MA) purification, resulting in solutions at final concentrations of ~5 µM in 50:50 methanol/water containing 0.1% formic acid. The instrument was externally calibrated using the Tuning Mix (Agilent, Santa Clara, CA).

2.2. ECD Experiments. ECD experiments were carried out on a Solarix 7 T FT-ICR mass spectrometer (Bruker, Billerica, MA) equipped with an Infinity cell and a nanoESI source operated in the positive ion mode. NanoESI emitters were pulled from quartz capillaries (O.D. = 1.0 mm and I.D. = 0.70 mm) with the use of a Sutter Instruments Co. P2000 laser puller (Sutter Instruments, Novato, CA). Sample aliquots (10 μ L of 5 μ M

solution) were loaded in a pulled-tip capillary, housed in a mounted custom built XYZ stage in front of the MS inlet, and voltages were applied via a tungsten wire inserted inside the nESI emitters. The nESI high voltage, capillary exit, and skimmers I and II were set to 1300 V, 200 V, 30 V and 4 V, respectively. Precursor ions were isolated in the instrument quadrupole with a mass window of 5 Da, accumulated for 0.5 s in the collision cell, and further injected into the ICR cell. ECD experiments were performed on the mass-selected [M+3H]³⁺ ions with a heated hollow cathode operating at a current of 1.5 A. Electrons emitted during 0.2 s were injected into the ICR cell with a 2.2 V bias and 10 V ECD lens. A total of 150 scans (m/z range 100-2000) were co-added with a data acquisition size of 512 K words.

2.3. TIMS-MS and CID Experiments. Ion mobility experiments were performed on a custom built nanoESI-TIMS coupled to an Impact Q-TOF mass spectrometer (Bruker, Billerica, MA, Figure S2) [50]. The TIMS unit is controlled using a custom software in LabView (National Instruments) synchronized with the MS platform controls [51]. NanoESI emitters were pulled from quartz capillaries (O.D. = 1.0 mm and I.D. = 0.70 mm) using a Sutter Instrument Co. P2000 laser puller (Sutter Instruments, Novato, CA). The general fundamentals of TIMS as well as the calibration procedure have been described previously [52-55]. Peptide sample solutions were loaded in a pulled-tip capillary, housed in a mounted custom built XYZ stage in front of the MS inlet, and sprayed at 950 V via a tungsten wire inserted inside the nESI emitters. TIMS-MS experiments were carried out using nitrogen (N₂) as buffer gas at room temperature. The gas velocity was kept constant between the funnel entrance ($P_1 = 2.6$ mbar) and exit (P_2 = 0.8 mbar, Figure S₂). An rf voltage of 250 V_{pp} at 880 kHz was applied to all electrodes. A voltage ramp (V_{ramp}) of -190 to -75 V, deflector voltage (V_{def}) of 60 V and base voltage (V_{out}) of 60 V were used for the mobility separations. Changes in the mobility profiles were not observed for the systems reported over 100-500 ms time range after desolvation. Collision induced dissociation (CID) experiments were performed in the collision cell located after the TIMS analyzer (Figure S2). The mass-selected [M+3H]³⁺ ions were fragmented using nitrogen as collision gas at a collision energy of 20-23 V. The mobility resolving power (*R*) values were determined as $R = CCS/\Delta CCS$, where ΔCCS is the full peak width at half maximum (FWHM) of the IMS band. A gaussian peak fitting

algorithm with non-linear least squares functions (Levenberg-Marquardt algorithm) using *OriginPro 2016* was used to evaluate the FWHM of each IMS band.

2.4. Correction of Pro substituted collision cross section (CCS). A direct comparison of the mobility profiles between the lanthipeptide Pcn2.8 and the [P8A], [P11A], [P12A], [P8A/P11A], [P8A/P12A], [P11A/P12A] and [P8A/P11A/P12A] variants was done by adjusting the CCS profiles based on methodology previously described [56-59]. Differences in CCS between N₂ and He were adjusted using the CCS_{N2} = 1.0857 (CCS_{He}) + 81.459 [Ų] equation [60,61]. This resulted in Pro to Ala substitutions to be corrected by 2.68 Ų in N₂.

3. RESULTS AND DISCUSSION

3.1. Fragmentation Pattern of Pcn2.8 in CID. The mass spectrometry analysis of the lanthipeptide Pcn2.8 resulted in the observation of doubly ($[M + 2H]^{2+}$, m/z 1025.9) and triply ($[M + 3H]^{3+}$, m/z 684.2) protonated species (Figure S₃). The CID analysis of the [M + 3H]³⁺ ions of Pcn2.8 (Figure 3a) exhibited multiple fragmentation patterns due to the presence of the thioether cross-links that prevent the formation of classic b_i/y_i fragment ions inside the ring. However, cross-linked product ions from b_i and y_i ions, denoted as $[(b_i)^-(y_i)]$, were observed. These fragments result from two bond cleavages in the thioether ring, yielding internal fragments denoted as $(b_i y_i)_n$, where the rest of the peptide remains covalently linked to the backbone through the thioether bond (Figure 3a). The main cross-linked product ions observed for Pcn2.8 were $[(b_{14})^{-}(y_1)]^{2+}$, $[(b_{14})^-(y_3)]^{2+}$, $[(b_{15})^-(y_2)]^{2+}$, and $[(b_{15})^-(y_3)]^{2+}$, associated with their complementary internal fragment ions $(b_{16}y_5)_4$, $(b_{16}y_5)_2$, $(b_{17}y_4)_2$, and $(b_{16}y_4)_1$, respectively. In addition, classic b_i/y_i series were observed, corresponding to fragmentations outside of the thioether rings (Figure 3a). The main product ions observed for Pcn2.8 were b_9^{2+} , b_{10}^{2+} , b_{11}^{2+} and b_{12}^{2+} series, together with their complementary y_{10} , y_{9} , y_{8} and y_{7} series. These fragments are located between the two thioether rings clearly evidencing the presence of a nonoverlapping lanthipeptide ring pattern, as previously described [25,28]. In fact, b_i/y_i series between the two thioether cross-links cannot be observed for the case of an overlapping lanthipeptide ring pattern because these linker residues are involved in the thioether ring (Figure S1). The cross-linked product ions were not observed for the previously reported MS/MS of Pcn2.8 using the $[M + 2H]^{2+}$ ions [25,28]. This observation

demonstrates that choosing the [M + 3H]³⁺ charge state as the precursor ion in CID allowed the detection of cross-linked fragment species and hence facilitates sequence coverage of lanthipeptides by delineating the residues present inside the thioether ring. A similar behavior has also been reported for the class I/III lasso peptides containing disulfide bonds [43,44].

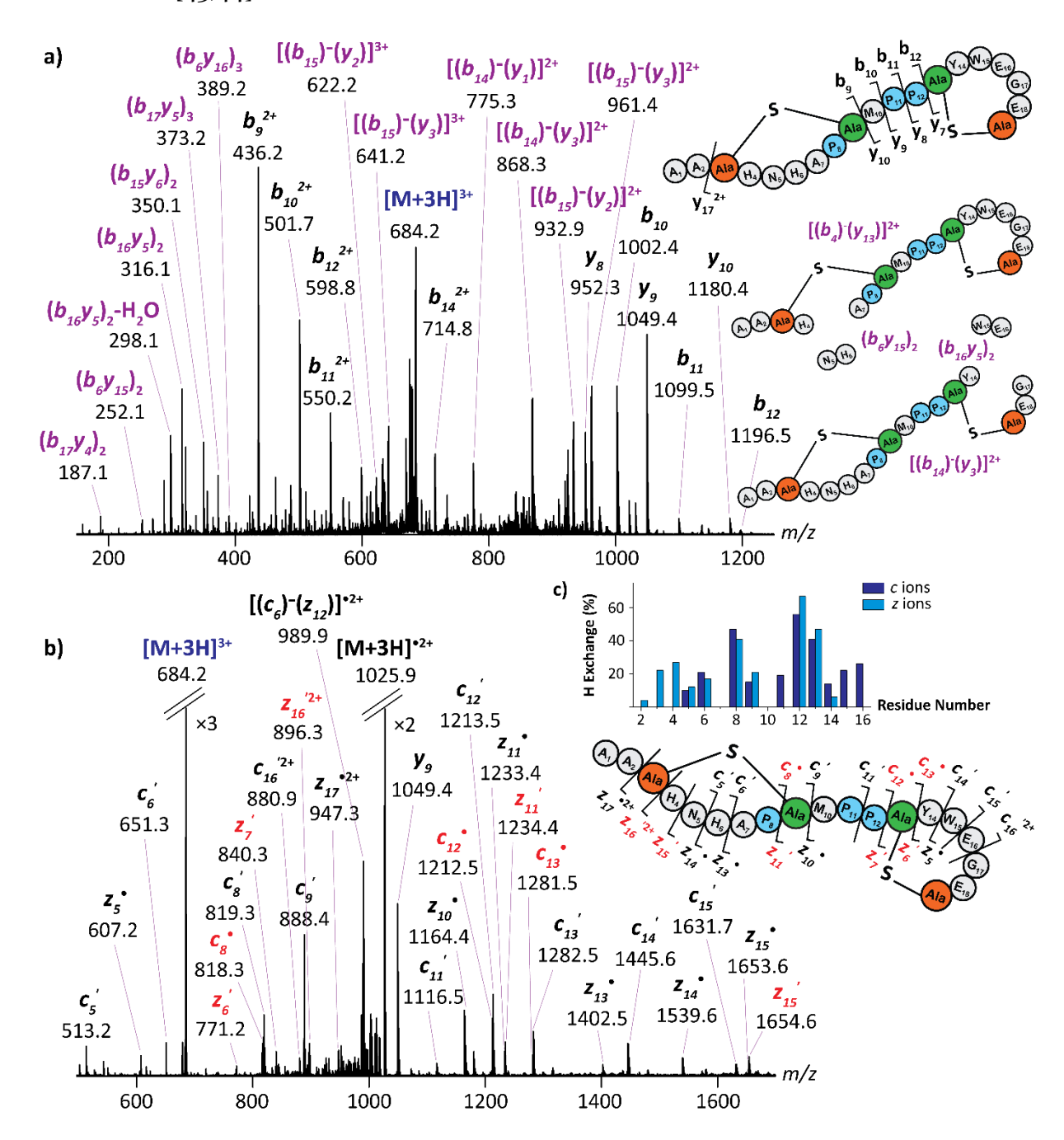


Figure 3. Typical tandem MS/MS spectra of the $[M + 3H]^{3+}$ ions of the lanthipeptide Pcn2.8 (m/z 684.2) using (a) CID and (b) ECD. The present CID and ECD spectra were generated using a collision energy of 23 V and a heated hollow cathode operating at a

current of 1.5 A, respectively. Typical cross-linked/internal fragments and hydrogen migration events are highlighted in purple and red, respectively, and labeled on the peptide cartoons (right of each panel). (c) Bar plot showing the hydrogen migration events of Pcn2.8 obtained by comparison between the experimental and theoretical isotopic patterns. The residues involved in the thioether cross-link are colored in orange (former Cys) and green (former Ser), respectively. The Pro residues are highlighted in blue.

3.2. Fragmentation Pattern of Pcn2.8 in ECD. We have previously illustrated the utility of ETD/ECD for the study of lasso peptides containing disulfide bonds as an alternative fragmentation approach to overcome potential limited structural information provided by CID [43,44]. The ETD/ECD processes involve the transfer/capture of a single electron that can induce dissociation in the backbone as well as in disulfide bonds [62-65]. ECD experiments were performed on the [M + 3H]3+ ions of Pcn2.8 yielding the spectrum presented in Figure 3b. The charge-reduced [M + 3H] $^{2+}$ ions (m/z 1025.9) were detected as the most abundant species. In addition, c_i'/z_i series were observed that involve the cleavage of the two thioether cross-links concomitant with backbone cleavages at each extremity of the thioether rings (Figure 3b). Here, we assume that the cleavage mechanism of thioether rings is similar to disulfide bonds. In fact, the cleavage of the $N-C_{\alpha}$ bond at the backbone region within the thioether bond occurs first, generating an intermediate radical that contains a radical site in the C_{α} atom, then followed by radical-driven reactions, where the C_{α} radical attacks the thioether bond, inducing cleavage at the S-C bond [62,66,65]. This results in the coverage of almost the entire lanthipeptide sequence and proves to be a more efficient approach than CID for the amino acid sequence elucidation. The cross-linked fragment ions generated by CID will probably not be detected when the size of the thioether ring becomes smaller, as observed for the lasso peptides [44]. Furthermore, ECD experiments of Pcn2.8 exhibited different hydrogen migration events when comparing the backbone residues with the residues involved as well as in close proximity of the thioether cross-links (Figure 3c). The c_{8} , c_{12} and c_{13} product ions were mass shifted by ~1 Da by the loss of H•, giving the c_{8} , c_{12} and c_{13} fragment ions, respectively (highlighted in red in Figure 3b). Conversely, the z_6 , z_{7} , z_{11} , z_{15} and z_{16} fragments were mass shifted by the capture of H•, giving the z_{6} , z_{7} ,

 z_{11} , z_{15} and z_{16} product ions, respectively (highlighted in red in Figure 3b). In addition, hydrogen migration events occurred less frequently when residues are located further away of the thioether cross-links (Figure 3c). Furthermore, larger extents of hydrogen migration were observed at the former Ser residues (highlighted in green) as compared to the former Cys residues (highlighted in orange). This suggests that ECD can assign which dSer/dThr residues are involved in thioether cross-links and therefore likely differentiate them from dSer/dThr residues not involved in a thioether for lanthipeptides where both are present. However, the assessment of the thioether ring connectivity remained ambiguous in ECD as compared to CID due to the cleavage of the thioether cross-links. As a consequence, the combination of both CID and ECD methods enabled to fully sequence Pcn2.8 as well as to firmly assess the lanthipeptide ring pattern. This analytical approach can be easily translated to other lanthipeptides and shows, like previously for lasso peptides [44,43], how CID and ECD of macrocyclic RiPPs complement each other.

3.3. TIMS-MS Analysis of Pcn2.8. TIMS-MS proved to be a very effective approach for the characterization of lasso peptides by providing additional information on the conformational diversity due to the high mobility resolving power of the TIMS analyzer [41,43,67]. TIMS spectra corresponding to the doubly and triply protonated species of Pcn2.8 are illustrated in Figures 4a and 4b, respectively. TIMS analysis for the [M + 2H]²⁺ and [M + 3H]3+ molecular species of Pcn2.8 resulted in the identification of a large number of IMS bands, with an apparent resolvin power of $R \sim 185$ and 155 using a Sr =0.23 V/ms, respectively. This observation suggests that the thioether cross-links probably prevent the lanthipeptide from completely collapsing toward compact structures, as reflected by the broad CCS distribution (> 50 Å2). In addition, the observation of a large conformational diversity suggests that the Pcn2.8 structure can be stabilized using several combinations of intramolecular interactions. For example, the absence of strong basic residues (e.g. Arg and Lys) can induce a competition in the protonation schemes, leading to different charge driven intramolecular interactions that will define a particular lanthipeptide structure. For example, one protonation scheme could preserve a rigid fold (compact structure) through charge solvation, possibly including salt bridges, bringing the residues involved in the two thioether cross-links in

proximity and stabilized by intramolecular hydrogen bonding interactions. An alternative scheme could include protonation that will pull apart the two thioether cross-links (extended structure) induced by Coulombic repulsions. This hypothesis is consistent with the recently reported electrostatic surface map of Pcn2.8 from its NMR structure, showing that the lanthipeptide neither has a preferred fold nor a specific charge organization on the surface of the peptide [29]. In addition, a particularity of Pcn2.8 is the presence of several Pro residues (Pro8, Pro11 and Pro12). This composition suggests that the conformational diversity can also be induced by *cis/trans*-isomerization of Pro residues, as previously observed for the lasso peptide microcin J25 [68]. In fact, the recent NMR study showed that Pcn2.8 can adopt two stable conformations, involving a *cis/trans*-equilibrium of the Ala7-Pro8 peptide bond while the Pro11 and Pro12 residues occupy only the *trans*-configurations [29].

Prochlorosin 2.8: [M+2H]²⁺ a) Sr 0.23 V/ms $R \sim 185$ 460 420 440 480 500 b) Prochlorosin 2.8: [M+3H]³⁺ Sr 0.23 V/ms $R \sim 155$ 550 500 600 450 650 CCS (Å²)

Figure 4. Typical TIMS spectra of the (a) doubly and (b) triply charged species of Pcn2.8. The former Cys and former Ser (Ala) residues that are involved in the thioether crosslinks are colored in orange and green, respectively. The Pro residues are highlighted in blue.

3.4. Evidence of *cis/trans*-Conformation at Pro8/Pro11/Pro12 Residues. The Pro8, Pro11 and Pro12 residues of Pcn2.8 were substituted with Ala residues through site-directed mutagenesis to assess the influence of possible *cis*-conformations at Pro

residues. These mutagenesis experiments resulted in the generation of the [P8A], [P11A], [P12A], [P8A/P11A], [P8A/P12A], [P11A/P12A] and [P8A/P11A/P12A] Pcn2.8 variants. The CID and ECD experiments using the $[M + 3H]^{3+}$ precursor ions of Pcn2.8 variants were consistent with the altered sequences for each variant (Figures S4 and S5). In addition, b_i/y_j product ions were observed by CID between the two thioether cross-links, demonstrating that the substitution by Ala residues does not affect the non-overlapping lanthipeptide ring pattern of Pcn2.8 (Figure S4). The ECD experiments also illustrated an alteration in the environment of the residues in close proximity of the thioether cross-links, as reflected by the changes observed in the hydrogen migration events (Figure S5). These observations suggest that each Pro residue plays an important role in the Pcn2.8 lanthipeptide structure.

TIMS-MS analysis of the investigated Pcn2.8 variants allowed the identification of the cis/trans-orientations of the proline state in wild type (WT) Pcn2.8 by direct comparison with the corrected mobility profiles (Table S1). The conservation or absence of an IMS band in the Pcn2.8 variants will then permit the assignment of the proline orientation in WT Pcn2.8, as previously reported for the lasso peptide microcin J25 [68]. High resolution TIMS analysis enabled the identification of fourteen IMS bands for the doubly protonated species of WT Pcn2.8 (Figure 5). In addition, distinct TIMS profiles were observed for WT Pcn2.8 and the Pcn2.8 variants, suggesting that the conformational diversity of WT Pcn2.8 involves cis/trans-conformations at proline residues (Table S1). TIMS distribution of the [P8A/P11A/P12A] variant, for which only trans-conformations are expected, indicated that the IMS bands 1, 3, 4, 5 and 7 correspond to trans-Pro8/trans-Pro11/trans-Pro12 (blue dashed lines in Figure 5). Note that these structures appeared to be the most compact structures in WT Pcn2.8, with the cis-conformation at Pro residues inducing then an unfolding event. The IMS 2 band (magenta dashed line in Figure 5) of WT Pcn2.8 was found common with only the [P8A/P11A] and [P8A/P12A] variants, indicating that the IMS 2 band probably involves only one proline (Pro11 or Pro12) in a cis-configuration, while the Pro8 residues adopts a trans-configuration. Thus, these observations suggest the presence of two possible structures with similar CCS for the IMS 2 band, involving a trans-Pro8/cis-Pro11/trans-Pro12 and/or a trans-Pro8/trans-Pro11/cis-Pro12. The IMS 6 band (red dashed line in

Figure 5) was only observed for the [P8A] variant concerning the single point mutation. This finding suggests the presence of a *trans*-Pro8/*cis*-Pro1/*cis*-Pro12 structure for the IMS 6 band. However, the IMS 6 band was also present for the [P8A/P1A], [P8A/P12A] and [P11A/P12A] variants, suggesting that structures including at least one of the prolines in a *cis*-configurations are observed. The IMS 8 band had a similar behavior as that of the IMS 6 band, for which the double mutations indicated that at least one of the prolines is in a *cis*-orientation, while the single point mutations pointed toward the presence of a *cis*-Pro8/*trans*-Pro11/*trans*-Pro12. The IMS 9, 10, 11 and 12 bands were generally observed in all Pcn2.8 variants, except for the [P8A/P11A/P12A] compound, for which only *trans*-configurations are observed, suggesting that these bands correspond to conformers in which at least one of the proline is in a *cis*-orientation (red dashed lines in Figure 5). The IMS 13 (purple dashed line) and 14 (green dashed line) bands were found unique for the [P11A] and [P12A] variants, respectively (Figure 5). This observation suggests that the IMS 13 band is specific for *cis*-Pro8/*trans*-Pro11/*cis*-Pro12, while the IMS 14 band is specific for *cis*-Pro8/*cis*-Pro11/*trans*-Pro12 (Table S1).

These TIMS results are in good agreement with recently reported NMR experiments [29], for which two populations involving a *cis/trans*-equilibrium of the Ala7-Pro8 peptide bond were observed. These NMR experiments were not able to decipher the Pro11 and Pro12 residues in a *cis*-orientation, probably because the *trans*-configuration at Pro11 and Pro12 are largely predominant in solution.

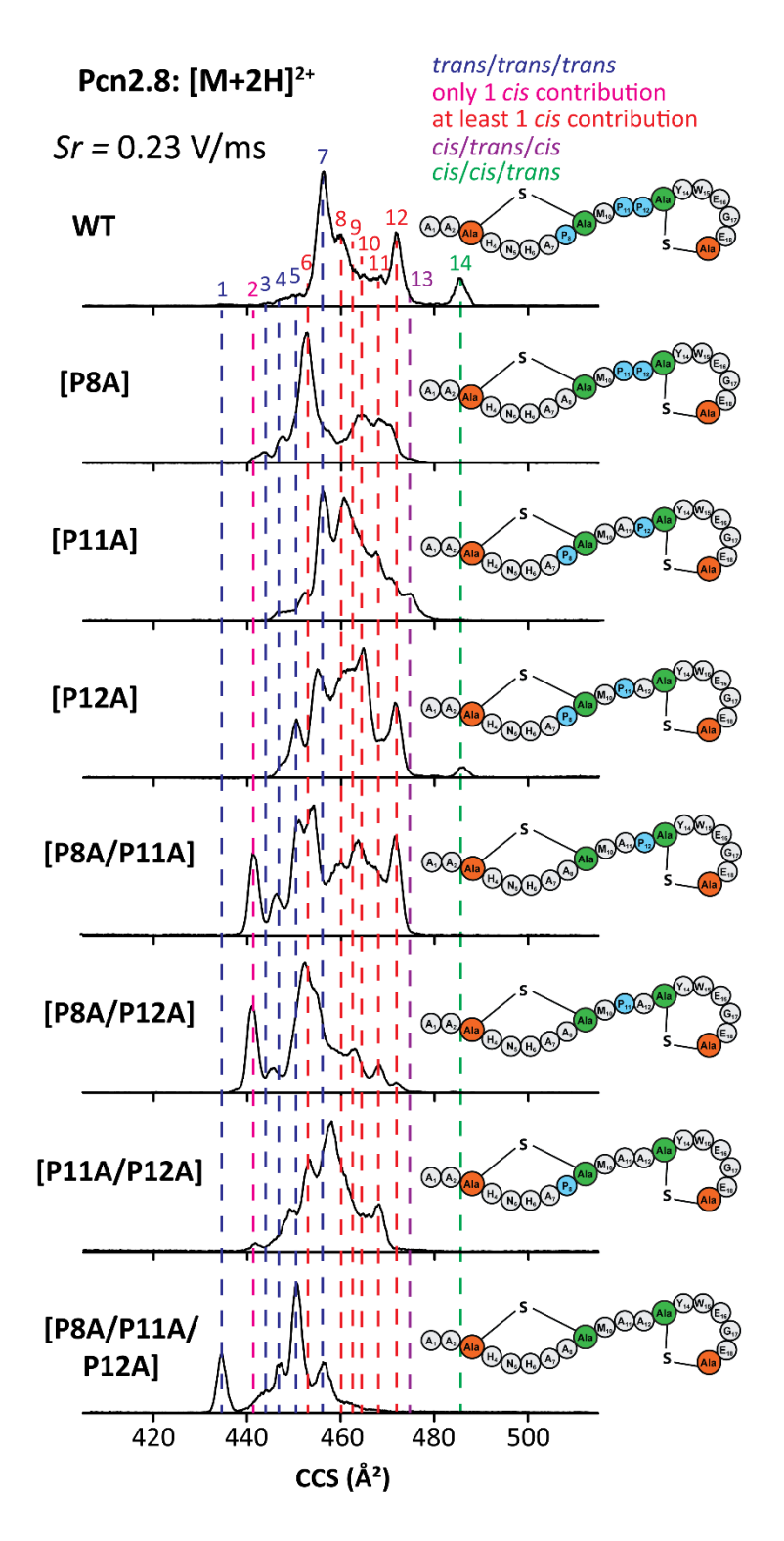


Figure 5. Typical TIMS spectra for the $[M + 2H]^{2+}$ ions of Pcn2.8 as well as the [P8A], [P11A] and [P12A] single variants, the [P8A/P11A], [P8A/P12A] and [P11A/P12A] double variants and the [P8A/P11A/P12A] triple variant. The CCS profiles of the mutants have been corrected for a direct IMS band comparison. The former Cys and former Ser residues that are involved in the thioether cross-links are colored in orange and green, respectively. The Pro residues are highlighted in blue.

4. CONCLUSION

Mass spectrometry based experiments were used to study the Pcn2.8 lanthipeptide structure and its potential ring patterns. The CID MS/MS experiments were found effective for the assignment of a non-overlapping lanthipeptide ring pattern by specifically yielding b_i and y_i fragments between the two thioether cross-links. The ECD MS/MS was effective to fully sequence the lanthipeptide by cleaving inside the thioether cross-links and by specifically showing larger extent of hydrogen migration near the residues involved in the thioether rings. The use of high-resolution mobility - mass spectrometry (TIMS-MS), in combination with site-directed mutagenesis ([P8A], [P11A], [P12A], [P8A/P11A], [P8A/P12A], [P11A/P12A] and [P8A/P11A/P12A] variants), permitted the identification of fourteen IMS bands, with varying prolines (Pro8, Pro11 and Pro12) in cis/trans-configurations. These observations provided complementary information to recent NMR findings, for which only the Pro8 residue was shown to adopt cis/transorientations. This study highlights the analytical power of the tandem MS/MS and TIMS-MS workflows for the structural characterization of lanthipeptides as a useful tool for a better understanding of the intramolecular forces that define the lanthipeptides folding motifs as well as the structural elements that drive the thioether cyclization process.

ACKNOWLEDGMENTS

The authors acknowledge the financial support from the National Science Foundation Division of Chemistry, under CAREER award CHE-1654274, with co-funding from the Division of Molecular and Cellular Biosciences to FFL and the National Institutes of Health (R₃₇ GMo₅8822) to WAV.

AUTHOR CONTRIBUTIONS

KJDF and JDH contributed equally to this work. The manuscript was written through contributions of all authors. All authors have given approval to the final version of the manuscript.

Conflict of Interest

The authors declare no competing financial interest.

REFERENCES

- 1. Arnison PG, Bibb MJ, Bierbaum G, Bowers AA, Bugni TS, Bulaj G, Camarero JA, Campopiano DJ, Challis GL, Clardy J, Cotter PD, Craik DJ, Dawson M, Dittmann E, Donadio S, Dorrestein PC, Entian KD, Fischbach MA, Garavelli JS, Goransson U, Gruber CW, Haft DH, Hemscheidt TK, Hertweck C, Hill C, Horswill AR, Jaspars M, Kelly WL, Klinman JP, Kuipers OP, Link AJ, Liu W, Marahiel MA, Mitchell DA, Moll GN, Moore BS, Muller R, Nair SK, Nes IF, Norris GE, Olivera BM, Onaka H, Patchett ML, Piel J, Reaney MJ, Rebuffat S, Ross RP, Sahl HG, Schmidt EW, Selsted ME, Severinov K, Shen B, Sivonen K, Smith L, Stein T, Sussmuth RD, Tagg JR, Tang GL, Truman AW, Vederas JC, Walsh CT, Walton JD, Wenzel SC, Willey JM, van der Donk WA (2013) Ribosomally synthesized and post-translationally modified peptide natural products: overview and recommendations for a universal nomenclature. Nat Prod Rep 30 (1):108-160. doi:10.1039/c2np20085f
- 2. Repka LM, Chekan JR, Nair SK, van der Donk WA (2017) Mechanistic Understanding of Lanthipeptide Biosynthetic Enzymes. Chem Rev 117 (8):5457-5520. doi:10.1021/acs.chemrev.6b00591
- 3. Knerr PJ, van der Donk WA (2012) Discovery, biosynthesis, and engineering of lantipeptides. Annu Rev Biochem 81:479-505. doi:10.1146/annurev-biochem-060110-113521
- 4. Ortiz-Lopez FJ, Carretero-Molina D, Sanchez-Hidalgo M, Martin J, Gonzalez I, Roman-Hurtado F, de la Cruz M, Garcia-Fernandez S, Reyes F, Deisinger JP, Muller A, Schneider T, Genilloud O (2020) Cacaoidin, First Member of the New Lanthidin RiPP Family. Angew Chem Int Ed 59 (31):12654-12658. doi:10.1002/anie.202005187
- 5. Xu M, Zhang F, Cheng Z, Bashiri G, Wang J, Hong J, Wang Y, Xu L, Chen X, Huang SX, Lin S, Deng Z, Tao M (2020) Functional Genome Mining Reveals a Class V Lanthipeptide Containing a d-Amino Acid Introduced by an F420 H2 -Dependent Reductase. Angew Chem Int Ed 59 (41):18029-18035. doi:10.1002/anie.202008035
- 6. Kloosterman AM, Cimermancic P, Elsayed SS, Du C, Hadjithomas M, Donia MS, Fischbach MA, van Wezel GP, Medema MH (2020) Expansion of RiPP biosynthetic space through integration of pangenomics and machine learning uncovers a novel class of lanthipeptides. PLoS Biol 18 (12):e3001026. doi:10.1371/journal.pbio.3001026
- 7. Zhang Q, Doroghazi JR, Zhao X, Walker MC, van der Donk WA (2015) Expanded natural product diversity revealed by analysis of lanthipeptide-like gene clusters in actinobacteria. Appl Environ Microbiol 81 (13):4339-4350. doi:10.1128/AEM.00635-15
- 8. Velasquez JE, van der Donk WA (2011) Genome mining for ribosomally synthesized natural products. Curr Opin Chem Biol 15 (1):11-21. doi:10.1016/j.cbpa.2010.10.027

- 9. Kersten RD, Yang YL, Xu Y, Cimermancic P, Nam SJ, Fenical W, Fischbach MA, Moore BS, Dorrestein PC (2011) A mass spectrometry-guided genome mining approach for natural product peptidogenomics. Nat Chem Biol 7 (11):794-802. doi:10.1038/nchembio.684
- 10. Mohimani H, Kersten RD, Liu WT, Wang M, Purvine SO, Wu S, Brewer HM, Pasa-Tolic L, Bandeira N, Moore BS, Pevzner PA, Dorrestein PC (2014) Automated genome mining of ribosomal peptide natural products. ACS Chem Biol 9 (7):1545-1551. doi:10.1021/cb500199h
- 11. Singh M, Sareen D (2014) Novel LanT associated lantibiotic clusters identified by genome database mining. PloS One 9 (3):e91352. doi:10.1371/journal.pone.0091352
- 12. Yang X, Lennard KR, He C, Walker MC, Ball AT, Doigneaux C, Tavassoli A, van der Donk WA (2018) A lanthipeptide library used to identify a protein-protein interaction inhibitor. Nat Chem Biol 14 (4):375-380. doi:10.1038/s41589-018-0008-5
- 13. Walker MC, Eslami SM, Hetrick KJ, Ackenhusen SE, Mitchell DA, van der Donk WA (2020) Precursor peptide-targeted mining of more than one hundred thousand genomes expands the lanthipeptide natural product family. BMC Genomics 21 (1):387. doi:10.1186/s12864-020-06785-7
- 14. Hegemann JD, van der Donk WA (2018) Investigation of Substrate Recognition and Biosynthesis in Class IV Lanthipeptide Systems. J Am Chem Soc 140 (17):5743-5754. doi:10.1021/jacs.8b01323
- 15. Hetrick KJ, Walker MC, van der Donk WA (2018) Development and Application of Yeast and Phage Display of Diverse Lanthipeptides. ACS Cent Sci 4 (4):458-467. doi:10.1021/acscentsci.7b00581
- 16. Urban JH, Moosmeier MA, Aumuller T, Thein M, Bosma T, Rink R, Groth K, Zulley M, Siegers K, Tissot K, Moll GN, Prassler J (2017) Phage display and selection of lanthipeptides on the carboxy-terminus of the gene-3 minor coat protein. Nat Commun 8 (1):1500. doi:10.1038/s41467-017-01413-7
- 17. Cotter PD, Deegan LH, Lawton EM, Draper LA, O'Connor PM, Hill C, Ross RP (2006) Complete alanine scanning of the two-component lantibiotic lacticin 3147: generating a blueprint for rational drug design. Mol Microbiol 62 (3):735-747. doi:10.1111/j.1365-2958.2006.05398.x
- 18. Montalban-Lopez M, Zhou L, Buivydas A, van Heel AJ, Kuipers OP (2012) Increasing the success rate of lantibiotic drug discovery by Synthetic Biology. Expert Opin Drug Discov 7 (8):695-709. doi:10.1517/17460441.2012.693476
- 19. Escano J, Smith L (2015) Multipronged approach for engineering novel peptide analogues of existing lantibiotics. Expert Opin Drug Discov 10 (8):857-870. doi:10.1517/17460441.2015.1049527 20. Sit CS, Yoganathan S, Vederas JC (2011) Biosynthesis of aminovinyl-cysteine-containing peptides and its application in the production of potential drug candidates. Acc Chem Res 44 (4):261-268. doi:10.1021/ar1001395

- 21. Namsolleck P, Richardson A, Moll GN, Mescheder A (2021) LP2, the first lanthipeptide GPCR agonist in a human pharmacokinetics and safety study. Peptides 136:170468. doi:10.1016/j.peptides.2020.170468
- 22. Kuipers A, Moll GN, Levy A, Krakovsky M, Franklin R (2020) Cyclic angiotensin-(1-7) contributes to rehabilitation of animal performance in a rat model of cerebral stroke. Peptides 123:170193. doi:10.1016/j.peptides.2019.170193
- 23. Bosma T, Rink R, Moosmeier MA, Moll GN (2019) Genetically Encoded Libraries of Constrained Peptides. ChemBioChem 20 (14):1754-1758. doi:10.1002/cbic.201900031
- 24. Yu Y, Mukherjee S, van der Donk WA (2015) Product Formation by the Promiscuous Lanthipeptide Synthetase ProcM is under Kinetic Control. J Am Chem Soc 137 (15):5140-5148. doi:10.1021/jacs.5b01409
- 25. Li B, Sher D, Kelly L, Shi Y, Huang K, Knerr PJ, Joewono I, Rusch D, Chisholm SW, van der Donk WA (2010) Catalytic promiscuity in the biosynthesis of cyclic peptide secondary metabolites in planktonic marine cyanobacteria. Proc Natl Acad Sci USA 107 (23):10430-10435. doi:10.1073/pnas.0913677107 26. Bobeica SC, van der Donk WA (2018) The Enzymology of Prochlorosin Biosynthesis. Methods Enzymol 604:165-203. doi:10.1016/bs.mie.2018.01.038
- 27. Tang W, van der Donk WA (2012) Structural characterization of four prochlorosins: a novel class of lantipeptides produced by planktonic marine cyanobacteria. Biochemistry 51 (21):4271-4279. doi:10.1021/bi300255s
- 28. Hegemann JD, Bobeica SC, Walker MC, Bothwell IR, van der Donk WA (2019) Assessing the Flexibility of the Prochlorosin 2.8 Scaffold for Bioengineering Applications. ACS Synth Biol 8 (5):1204-1214. doi:10.1021/acssynbio.9b00080
- 29. Bobeica SC, Zhu L, Acedo JZ, Tang W, van der Donk WA (2020) Structural determinants of macrocyclization in substrate-controlled lanthipeptide biosynthetic pathways. Chem Sci. doi:10.1039/d0sc01651a
- 30. Chan WC, Bycroft BW, Leyland ML, Lian L-Y, Yang JC, Roberts GCK (1992) Sequence-specific resonance assignment and conformational analysis of subtilin by 2D NMR. FEBS Lett 300 (1):56-62. doi:10.1016/0014-5793(92)80163-b
- 31. Moon K, Xu F, Seyedsayamdost MR (2019) Cebulantin, a Cryptic Lanthipeptide Antibiotic Uncovered Using Bioactivity-Coupled HiTES. Angew Chem Int Ed 58 (18):5973-5977. doi:10.1002/anie.201901342
- 32. Hsu ST, Breukink E, Tischenko E, Lutters MA, de Kruijff B, Kaptein R, Bonvin AM, van Nuland NA (2004) The nisin-lipid II complex reveals a pyrophosphate cage that provides a blueprint for novel antibiotics. Nat Struct Mol Biol 11 (10):963-967. doi:10.1038/nsmb830

- 33. Shenkarev ZO, Finkina EI, Nurmukhamedova EK, Balandin SV, Mineev KS, Nadezhdin KD, Yakimenko ZA, Tagaev AA, Temirov YV, Arseniev AS, Ovchinnikova TV (2010) Isolation, structure elucidation, and synergistic antibacterial activity of a novel two-component lantibiotic lichenicidin from Bacillus licheniformis VK21. Biochemistry 49 (30):6462-6472. doi:10.1021/bi100871b
- 34. Vasile F, Potenza D, Marsiglia B, Maffioli S, Donadio S (2012) Solution structure by nuclear magnetic resonance of the two lantibiotics 97518 and NAI-107. J Pept Sci 18 (2):129-134. doi:10.1002/psc.1425
- 35. Garg N, Tang W, Goto Y, Nair SK, van der Donk WA (2012) Lantibiotics from Geobacillus thermodenitrificans. Proc Natl Acad Sci USA 109 (14):5241-5246. doi:10.1073/pnas.1116815109
- 36. Zhang J, Feng Y, Teng K, Lin Y, Gao Y, Wang J, Zhong J (2014) Type AII lantibiotic bovicin HJ50 with a rare disulfide bond: structure, structure-activity relationships and mode of action. Biochem J 461 (3):497-508. doi:10.1042/BJ20131524
- 37. Lohans CT, Li JL, Vederas JC (2014) Structure and biosynthesis of carnolysin, a homologue of enterococcal cytolysin with D-amino acids. J Am Chem Soc 136 (38):13150-13153. doi:10.1021/ja5070813
- 38. Fujinami D, Mahin AA, Elsayed KM, Islam MR, Nagao JI, Roy U, Momin S, Zendo T, Kohda D, Sonomoto K (2018) The lantibiotic nukacin ISK-1 exists in an equilibrium between active and inactive lipid-II binding states. Commun Biol 1:150. doi:10.1038/s42003-018-0150-3
- 39. Karczewski J, Krasucki SP, Asare-Okai PN, Diehl C, Friedman A, Brown CM, Maezato Y, Streatfield SJ (2020) Isolation, Characterization and Structure Elucidation of a Novel Lantibiotic From Paenibacillus sp. Front Microbiol 11:598789. doi:10.3389/fmicb.2020.598789
- 40. Zhang Q, Ortega M, Shi Y, Wang H, Melby JO, Tang W, Mitchell DA, van der Donk WA (2014) Structural investigation of ribosomally synthesized natural products by hypothetical structure enumeration and evaluation using tandem MS. Proc Natl Acad Sci USA 111 (33):12031-12036. doi:10.1073/pnas.1406418111
- 41. Jeanne Dit Fouque K, Moreno J, Hegemann JD, Zirah S, Rebuffat S, Fernandez-Lima F (2018) Identification of Lasso Peptide Topologies Using Native Nanoelectrospray Ionization-Trapped Ion Mobility Spectrometry-Mass Spectrometry. Anal Chem 90 (8):5139-5146. doi:10.1021/acs.analchem.7b05230
- 42. Fouque KJ, Lavanant H, Zirah S, Hegemann JD, Zimmermann M, Marahiel MA, Rebuffat S, Afonso C (2017) Signatures of Mechanically Interlocked Topology of Lasso Peptides by Ion Mobility-Mass Spectrometry: Lessons from a Collection of Representatives. J Am Soc Mass Spectrom 28 (2):315-322. doi:10.1007/s13361-016-1524-8
- 43. Jeanne Dit Fouque K, Bisram V, Hegemann JD, Zirah S, Rebuffat S, Fernandez-Lima F (2019) Structural signatures of the class III lasso peptide BI-32169 and the branched-cyclic topoisomers using

- trapped ion mobility spectrometry-mass spectrometry and tandem mass spectrometry. Anal Bioanal Chem 411 (24):6287-6296. doi:10.1007/s00216-019-01613-8
- 44. Jeanne Dit Fouque K, Lavanant H, Zirah S, Hegemann JD, Fage CD, Marahiel MA, Rebuffat S, Afonso C (2018) General rules of fragmentation evidencing lasso structures in CID and ETD. Analyst 143 (5):1157-1170. doi:10.1039/c7an02052j
- 45. Zirah S, Afonso C, Linne U, Knappe TA, Marahiel MA, Rebuffat S, Tabet J-C (2011) Topoisomer Differentiation of Molecular Knots by FTICR MS: Lessons from Class II Lasso Peptides. J Am Soc Mass Spectrom 22 (3):467-479. doi:10.1007/s13361-010-0028-1
- 46. Perot-Taillandier M, Zirah S, Rebuffat S, Linne U, Marahiel MA, Cole RB, Tabet JC, Afonso C (2012) Determination of peptide topology through time-resolved double-resonance under electron capture dissociation conditions. Anal Chem 84 (11):4957-4964. doi:10.1021/ac300607y
- 47. Bobeica SC, Dong SH, Huo L, Mazo N, McLaughlin MI, Jimenez-Oses G, Nair SK, van der Donk WA (2019) Insights into AMS/PCAT transporters from biochemical and structural characterization of a double Glycine motif protease. eLife 8. doi:10.7554/eLife.42305
- 48. Chiu J, March PE, Lee R, Tillett D (2004) Site-directed, Ligase-Independent Mutagenesis (SLIM): a single-tube methodology approaching 100% efficiency in 4 h. Nucleic Acids Res 32 (21):e174. doi:10.1093/nar/gnh172
- 49. Chiu J, Tillett D, Dawes IW, March PE (2008) Site-directed, Ligase-Independent Mutagenesis (SLIM) for highly efficient mutagenesis of plasmids greater than 8kb. J Microbiol Methods 73 (2):195-198. doi:10.1016/j.mimet.2008.02.013
- 50. Fernandez-Lima FA, Kaplan DA, Suetering J, Park MA (2011) Gas-phase separation using a Trapped Ion Mobility Spectrometer. Int J Ion Mobil Spectrom 14 (2-3):93-98
- 51. Fernandez-Lima FA, Kaplan DA, Park MA (2011) Note: Integration of trapped ion mobility spectrometry with mass spectrometry. Rev Sci Instrum 82 (12):126106. doi:10.1063/1.3665933
- 52. Hernandez DR, Debord JD, Ridgeway ME, Kaplan DA, Park MA, Fernandez-Lima F (2014) Ion dynamics in a trapped ion mobility spectrometer. Analyst 139 (8):1913-1921. doi:10.1039/c3an02174b
- 53. Ridgeway ME, Lubeck M, Jordens J, Mann M, Park MA (2018) Trapped ion mobility spectrometry: A short review. Int J Mass Spectrom 425:22-35. doi:10.1016/j.ijms.2018.01.006
- 54. Silveira JA, Michelmann K, Ridgeway ME, Park MA (2016) Fundamentals of Trapped Ion Mobility Spectrometry Part II: Fluid Dynamics. J Am Soc Mass Spectrom 27 (4):585-595. doi:10.1007/s13361-015-1310-z
- 55. Michelmann K, Silveira JA, Ridgeway ME, Park MA (2015) Fundamentals of trapped ion mobility spectrometry. J Am Soc Mass Spectrom 26 (1):14-24. doi:10.1007/s13361-014-0999-4
- 56. Pierson NA, Chen L, Russell DH, Clemmer DE (2013) Cis-trans isomerizations of proline residues are key to bradykinin conformations. J Am Chem Soc 135 (8):3186-3192. doi:10.1021/ja3114505

- 57. Dilger JM, Valentine SJ, Glover MS, Ewing MA, Clemmer DE (2012) A database of alkali metal-containing peptide cross sections: Influence of metals on size parameters for specific amino acids. Int J Mass Spectrom 330:35-45. doi:10.1016/j.ijms.2012.05.001
- 58. Valentine SJ, Counterman AE, Clemmer DE (1999) A database of 660 peptide ion cross sections: Use of intrinsic size parameters for bona fide predictions of cross sections. J Am Soc Mass Spectrom 10 (11):1188-1211. doi:Doi 10.1016/S1044-0305(99)00079-3
- 59. Srebalus Barnes CA, Clemmer DE (2003) Assessing Intrinsic Side Chain Interactions between i and i + 4 Residues in Solvent-Free Peptides: A Combinatorial Gas-Phase Approach. J Phys Chem A 107 (49):10566-10579. doi:10.1021/jp030519s
- 60. Bush MF, Hall Z, Giles K, Hoyes J, Robinson CV, Ruotolo BT (2010) Collision cross sections of proteins and their complexes: a calibration framework and database for gas-phase structural biology. Anal Chem 82 (22):9557-9565. doi:10.1021/ac1022953
- 61. Bush MF, Campuzano ID, Robinson CV (2012) Ion mobility mass spectrometry of peptide ions: effects of drift gas and calibration strategies. Anal Chem 84 (16):7124-7130. doi:10.1021/ac3014498
- 62. Cole SR, Ma X, Zhang X, Xia Y (2012) Electron transfer dissociation (ETD) of peptides containing intrachain disulfide bonds. J Am Soc Mass Spectrom 23 (2):310-320. doi:10.1007/s13361-011-0300-z
- 63. Clark DF, Go EP, Desaire H (2013) Simple approach to assign disulfide connectivity using extracted ion chromatograms of electron transfer dissociation spectra. Anal Chem 85 (2):1192-1199. doi:10.1021/ac303124w
- 64. Zubarev RA, Kruger NA, Fridriksson EK, Lewis MA, Horn DM, Carpenter BK, McLafferty FW (1999) Electron Capture Dissociation of Gaseous Multiply-Charged Proteins Is Favored at Disulfide Bonds and Other Sites of High Hydrogen Atom Affinity. J Am Chem Soc 121 (12):2857-2862. doi:10.1021/ja981948k
- 65. Ganisl B, Breuker K (2012) Does Electron Capture Dissociation Cleave Protein Disulfide Bonds? ChemistryOpen 1 (6). doi:10.1002/open.201200038
- 66. Asakawa D, Takahashi H, Iwamoto S, Tanaka K (2019) Hydrogen attachment dissociation of peptides containing disulfide bonds. Phys Chem Chem Phys 21 (47):26049-26057. doi:10.1039/c9cp03923f
- 67. Jeanne Dit Fouque K, Moreno J, Hegemann JD, Zirah S, Rebuffat S, Fernandez-Lima F (2018) Metal ions induced secondary structure rearrangements: mechanically interlocked lasso vs. unthreaded branched-cyclic topoisomers. Analyst 143 (10):2323-2333. doi:10.1039/c8an00138c
- 68. Jeanne Dit Fouque K, Hegemann JD, Zirah S, Rebuffat S, Lescop E, Fernandez-Lima F (2019) Evidence of Cis/Trans-Isomerization at Pro7/Pro16 in the Lasso Peptide Microcin J25. J Am Soc Mass Spectrom 30 (6):1038-1045. doi:10.1007/s13361-019-02134-5

FIGURES

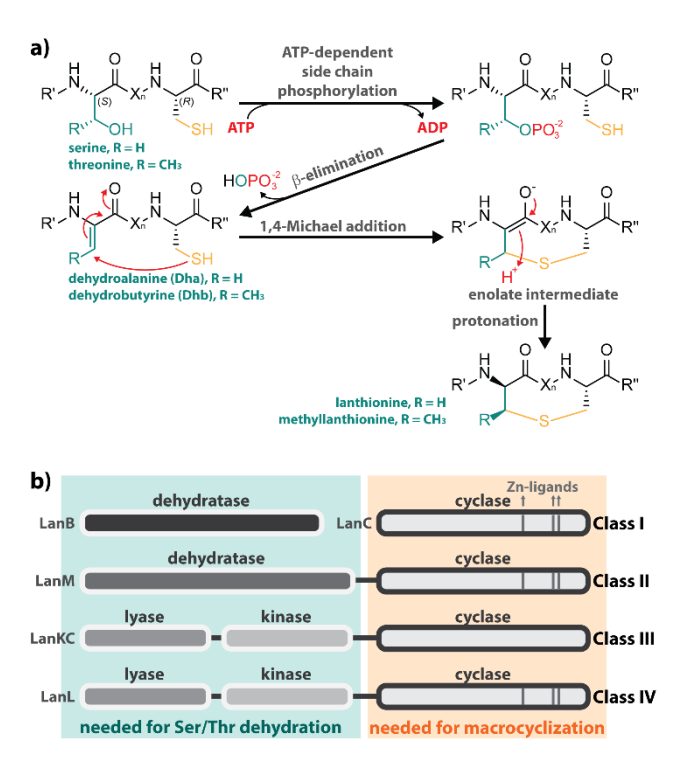


Figure 1. (a) Mechanisms of the lanthipeptide biosynthesis, starting with a dehydratation of Ser/Thr residues, followed by a cyclization through nucleophilic attack of Cys thiol groups. (b) General classification of lanthipeptide processing enzymes. The details of the recently reported class V lanthipeptides have not yet been worked out.

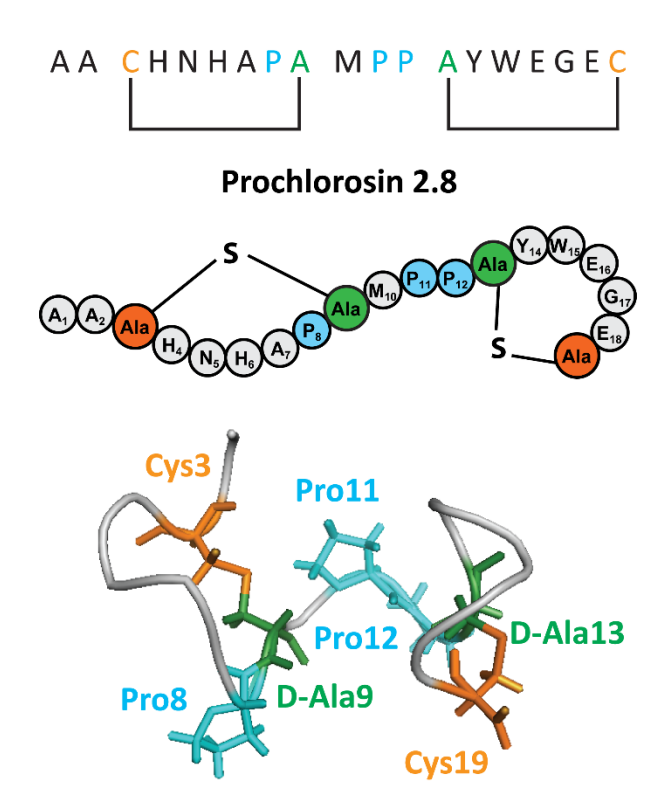


Figure 2. Sequence, schematic and 3D representation (pdb: 6VLJ [29]) of the lanthipeptide prochlorosin 2.8. The Cys and dSer residues, involved in the thioether cross-link formation, are colored in orange and green, respectively. The Pro residues are highlighted in blue.

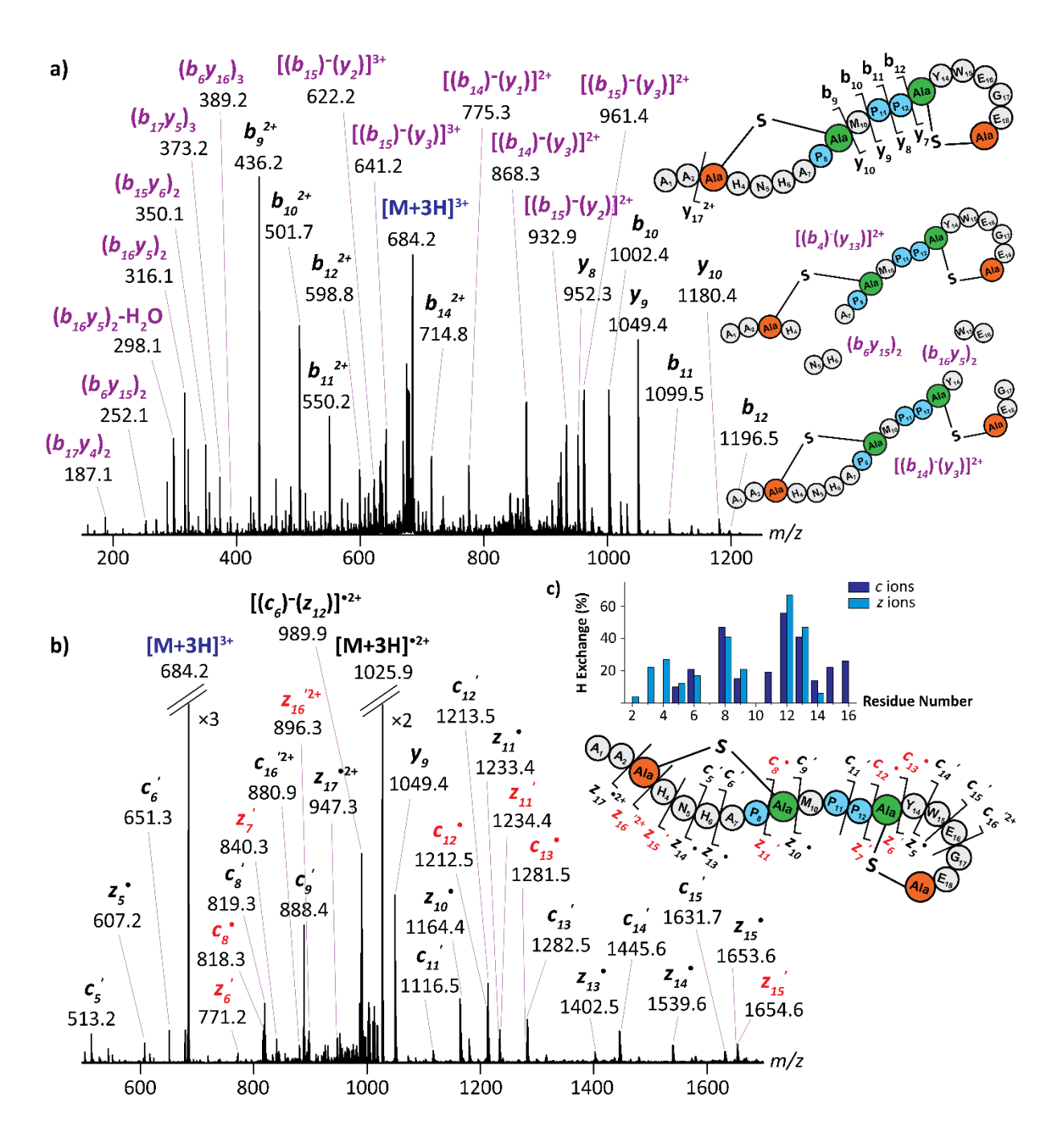


Figure 3. Typical tandem MS/MS spectra of the $[M + 3H]^{3+}$ ions of the lanthipeptide Pcn2.8 (m/z 684.2) using (a) CID and (b) ECD. Typical cross-linked/internal fragments and hydrogen migration events are highlighted in purple and red, respectively, and labeled on the peptide cartoons (right of each panel). (c) Bar plot showing the hydrogen migration events of Pcn2.8 obtained by comparison between the experimental and theoretical isotopic patterns. The residues involved in the thioether cross-link are colored in orange (former Cys) and green (former Ser), respectively. The Pro residues are highlighted in blue.

a) Prochlorosin 2.8: [M+2H]²⁺ Sr 0.23 V/ms $R \sim 185$ 420 460 440 480 500 b) Prochlorosin 2.8: [M+3H]³⁺ Sr 0.23 V/ms *R* ~ 155 500 550 600 450 650 CCS (Å²)

Figure 4. Typical TIMS spectra of the (a) doubly and (b) triply charged species of Pcn2.8. The former Cys and former Ser (Ala) residues that are involved in the thioether crosslinks are colored in orange and green, respectively. The Pro residues are highlighted in blue.

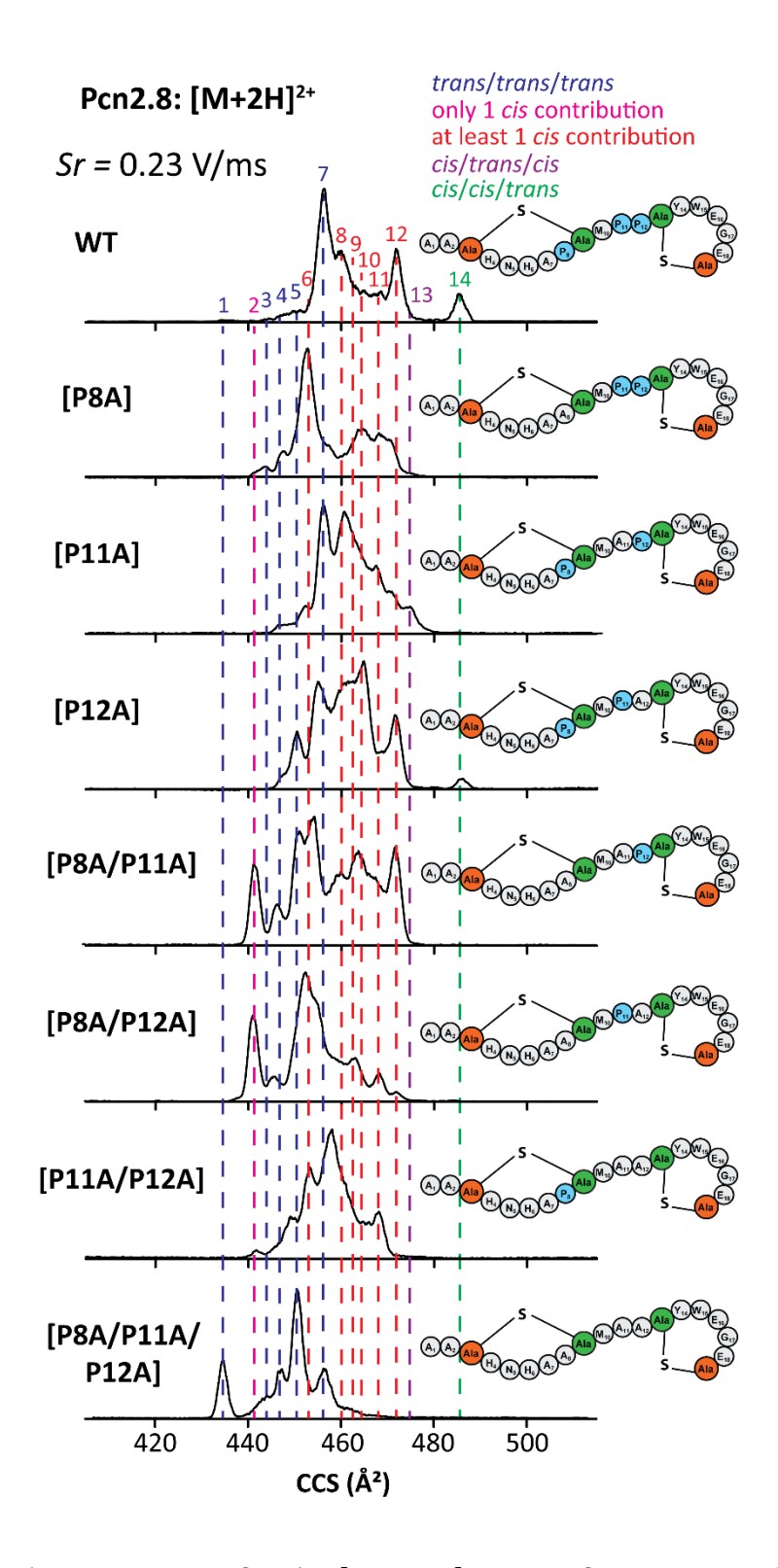
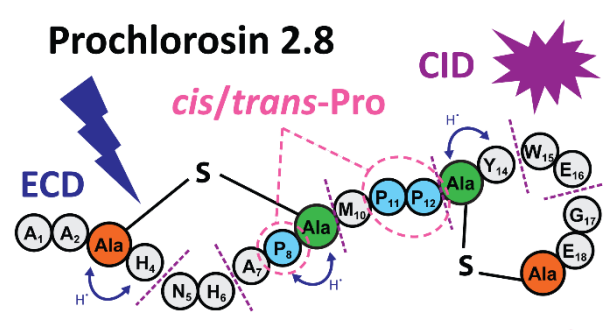


Figure 5. Typical TIMS spectra for the [M + 2H]²⁺ ions of Pcn2.8 as well as the [P8A], [P11A] and [P12A] single variants, the [P8A/P11A], [P8A/P12A] and [P11A/P12A] double variants and the [P8A/P11A/P12A] triple variant. The CCS profiles of the mutants have been corrected for a direct IMS band comparison. The former Cys and former Ser residues that are involved in the thioether cross-links are colored in orange and green, respectively. The Pro residues are highlighted in blue.

GRAPHICAL ABSTRACT



TIMS - Mutagenesis